Oncology Research, Vol. 28, pp. 745–761
Printed in the USA.

0965-0407/21 $90.00 + .00
DOI: https://doi.org/10.3727/096504021X16130322409507
E-ISSN 1555-3906
www.cognizantcommunication.com

Therapeutic Targeting PLK1 by ON-01910.Na Is Effective in Local Treatment of Retinoblastoma

Huan Ma,[1] Cong Nie,[1] Ying Chen, Jinmiao Li, Yanjie Xie, Zhixin Tang, Yang Gao, Siming Ai, Yuxiang Mao, Qian Sun, and Rong Lu

State Key Laboratory of Ophthalmology, Zhongshan Ophthalmic Center, Sun Yat-Sen University, Guangzhou, P.R. China

Cell cycle deregulation is involved in the pathogenesis of many cancers and is often associated with protein kinase aberrations, including the polo-like kinase 1 (PLK1). We used retinoblastoma, an intraocular malignancy that lacks targeted therapy, as a disease model and set out to reveal targetability of PLK1 with a small molecular inhibitor ON-01910.Na. First, transcriptomic analysis on patient retinoblastoma tissues suggested that cell cycle progression was deregulated and confirmed that PLK1 pathway was upregulated. Next, antitumor activity of ON-01910.Na was investigated in both cellular and animal levels. Cytotoxicity induced by ON-01910.Na was tumor specific and dose dependent in retinoblastoma cells, while nontumor cells were minimally affected. In three-dimensional culture, ON-01910.Na demonstrated efficient drug penetrability with multilayer cell death. Posttreatment transcriptomic findings revealed that cell cycle arrest and MAPK cascade activation were induced following PLK1 inhibition and eventually resulted in apoptotic cell death. In Balb/c nude mice, a safe threshold of 0.8 nmol intravitreal dosage of ON-01910.Na was established for intraocular safety, which was demonstrated by structural integrity and functional preservation. Furthermore, intraocular and subcutaneous xenograft were significantly reduced with ON-01910.Na treatments. For the first time, we demonstrated targetability of PLK1 in retinoblastoma by efficiently causing cell cycle arrest and apoptosis. Our study is supportive that local treatment of ON-01910.Na may be a novel, effective modality benefiting patients with PLK1-aberrant tumors.

Key words: Retinoblastoma; PLK1 signaling pathway; MAPK signaling pathway; ON-01910.Na; Targeted therapy; Retina safety

INTRODUCTION

It is generally acknowledged that tumorigenesis is initiated by consistent inactivation or deletion of tumor suppressor genes, which often have regulatory roles in the cell cycle and cell proliferation[1]. Classic tumor suppressor genes include *RB1*, *TP53*, and *PTEN*, and their genomic changes have been found associated with drug resistance and poorer prognosis in many types of cancers[2,3]. *RB1*, which encodes protein "retinoblastoma" (pRB), is the first tumor suppressor discovered in humans and is best known as a fundamental housekeeper involved in cell cycle regulation[4,5]. pRB inhibits cell proliferation by forming a complex with E2F transcription factors and constraining binding of target promoters[6], and loss or deactivation of pRB results in constant cell cycle progression from the G_1 to the S phase[7].

The vicious circle of aberrant progress of cell cycle, chromosomal instability, accumulation of mutations, and pro-oncogenic activities collectively drive toward malignant transformation[8,9]. Current strategies of precision therapy lay on the likelihood of targeting the highly active oncogenes, which is easier than restoring the function of inactivated tumor suppressors[3]. The cell cycle network is regulated by many protein kinases, and many are now recognized as oncogenic in tumorigenesis. To date, targeting protein kinases in anticancer medicine has gained successful achievements in many cancer types[10,11].

Polo-like kinase 1 (PLK1) is an important factor that is crucially involved in the control of cell division and has multiple roles in regulation of the cell cycle network[12,13]. PLK1 is oncogenic as it has been shown as overexpressed and of prognostic significance in a wide range of malignancies such as non-small cell lung cancers, esophageal cancers, and melanomas[14–16]. ON-01910.Na, a synthetic novel benzyl styryl sulfone also known as rigosertib, is a small-molecule inhibitor that targets PLK1 currently

[1]These authors provided equal contribution to this work.
Address correspondence to Rong Lu, M.D., Ph.D., State Key Laboratory of Ophthalmology, Zhongshan Ophthalmic Center, Sun Yat-Sen University, 54 Xianlie S. Road, Guangzhou 510060, P.R. China. Tel: +86 20 87331539; E-mail: lurong@gzzoc.com

considered as a readily accessible therapeutic strategy against certain cancers such as leukemia and non-small cell lung cancers[17–19]. ON-01910.Na mimetically binds to the Ras-binding region of various Ras effector proteins and subsequently imposes inhibitory effect to polo-like kinase (PLK) and phosphoinositide-3-kinase (PI3K) pathways[20].

Numerous diseases and cancers are associated with deregulated cell cycle due to defected *RB1*, including the naming disease retinoblastoma (RB) itself. RB is a life-threatening pediatric malignancy that has a low morbidity of 1 per 18,000 live births globally[21]. Current local therapy for RB may result in ocular toxicity due to nonspecificity for tumor[22,23], yet there has not been an effective targeted therapy including the cell cycle. RB is characterized by biallelic inactivation of *RB1*, leading to speculation of the tumorigenic role of deregulated cell cycle. In one of our previous studies[24], we found that the pathways associated with cell cycle and cell division were mostly enriched with differentially expressed genes identified between RB and normal retina tissues. Furthermore, the upregulated hub genes with higher degree values such as *CDK1*, *CCNB1*, *BUB1*, and *AURKA* were closely related to the PLK1 signaling pathway in the cell cycle network. Therefore, RB is a well-suited disease model for our interest to investigate the targetability of PLK1 and cell cycle.

Our work is the first to investigate the translational applicability of PLK1-selective compound in treatment for RB. Transcriptomic analysis was performed on RB tissues, and our findings emphasized the importance of cell cycle progression. We anticipate that cell cycle deregulation in RB is correlated with aberrant protein kinases. In this study, we assessed PLK1 targetability in RB, and we performed preclinical investigation of ON-01910.Na, a small-molecule inhibitor, with locally confined administration.

MATERIALS AND METHODS

Patient Sample Collection

Fresh human RB samples were obtained from patients with unilateral group E tumors who underwent enucleation at Zhongshan Ophthalmic Center (ZOC), Sun Yat-Sen University, Guangzhou, P.R. China. Fresh retinas were provided by the Guangdong Eye Bank. Ethical approval and patient consents were obtained before surgery, and procedures adhered to the tenets of the 1964 Declaration of Helsinki. Protocols were approved by institutional review boards at ZOC.

Cell Culture and Drug Treatments

Primary, patient-derived RB cells were isolated from freshly harvested RB tissues with a protocol previously described, and grown under a serum-free composite of Dulbecco's modified Eagle's medium (DMEM)/F12 (Gibco, ThermoFisher Scientific, Waltham, MA, USA)[25]. Two RB cell lines, Weri-RB1 and Y79, and a nontumor human retinal pigment epithelial cell line ARPE-19 (American Type Culture Collection, Manassas, VA, USA) were grown according to the supplier's recommendations. All cell lines used in this study were authenticated with human short tandem repeat (STR) profiling.

Drug chemicals used in this study include small-molecule inhibitors such as PLK1 inhibitor ON-01910.Na, p38 mitogen-activated protein kinase (MAPK) inhibitor BMS-582949 HCl, c-Jun N-terminal kinase (JNK) inhibitor SP600125, and extracellular signal-regulated kinase 1/2 (ERK1/2) inhibitor SCH772984. Alkylating agent melphalan was used as efficacy reference. All chemicals were acquired from MedChem Express (Princeton, NJ, USA). All drug chemicals were dissolved, and concentrations were made up in solvent dimethyl sulfoxide (DMSO); the final applied volume did not exceed 0.1% of total medium volume. Drug- and vehicle-treated cells have undergone cytotoxicity and viability assessments, flow cytometry for apoptosis and cell cycle analyses, and transcriptome sequencing. For investigation on MAPK signaling pathway, cells were treated simultaneously with MAPK inhibitors and PLK1 inhibitor ON-01910.Na.

Transcriptome Sequencing and Bioinformatic Analyses

Total RNA was extracted from RB tissues and ON-01910.Na-/vehicle-treated cells (Weri-RB1, Y79, and ARPE-19) for whole transcriptomic high-throughput sequencing (RNA-seq), accomplished by the Beijing Genomics Institute (BGI) Company (Shenzhen, P.R. China). Fragments per kilobase of transcript per million fragments mapped obtained in RNA sequencing analysis were log2 transformed and applied in sequential bioinformatic analyses, including Kyoto Encyclopedia of Genes and Genomes (KEGG) pathway enrichment analysis, STRING database for protein–protein interaction (PPI) network analysis, screening through the CytoHubba program (Cytoscape, http://cytoscape.org/), UALCAN database for The Cancer Genome Atlas (TCGA) search, and Gene Expression Profiling Interactive Analysis (GEPIA) analysis. RNA sequencing data from three fresh normal retinas were used as reference data.

Cell Viability Assay

Cell viabilities of RB cells (Weri-RB1 and Y79, and patient-derived cells) and nontumor ARPE-19 after drug applications were assessed using the Cell Counting Kit-8 (CCK-8) MTT assay (KeyGEN BioTECH, Jiangsu, P.R. China) according to the manufacturer's instruction. ON-01910.Na, melphalan, or vehicle 10% DMSO was directly applied to cell culture 24 to 96 h prior to CCK-8 assessment. For each concentration of drug application,

three wells were assessed in each run to obtain an average value, and three independent runs were performed. With triplications of the assays, data were confirmed with consistency.

Cytotoxicity in Three-Dimensional (3D) RB Culture

Protocol for 3D spherical culture of patient-derived primary RB cells was modified from organoid culture described previously[26]. Above described serum-free composite of DMEM/F12 was used. Treatment was performed by replacing growth medium with freshly prepared medium loaded with 4 μM ON-01910.Na or melphalan, or vehicle DMSO. Effect of the time length of exposure was assessed at various time points: 12, 24, 36, 48, 72, and 96 h. Cytotoxicity in spherical culture was assessed by addition of 10% typan blue dye and visualized under an inverted light-field microscope. Typan blue intensity indicates the extent of drug penetration into the tumor spheroids, and stain intensities were scaled and labeled with three colors: green (live), magenta, and red (cell death, with increasing overlay of dead cells). Proportion of dead/live cells was estimated by area in 2D planar.

Assessment of Apoptosis and Cell Cycle by Flow Cytometry

Annexin V–fluorescein isothiocyanate (FITC)/propidium iodide (PI) kits (KeyGEN BioTECH) was used for assessment of apoptosis under the effect of drugs for 24 h using the manufacturer's instruction. Analysis on cell cycle alterations under drug effect for 24 h was performed with the Cell Cycle Assessment Kit (KeyGEN BioTECH) following the manufacturer's instruction. Flow cytometry analysis was performed using a BD LSR Fortessa Flow Cytometer (BD Biosciences, San Jose, CA, USA). Apoptotic analysis data were analyzed with ModFit LT software (version 5.0.9, Verity Software House, Topsham, ME, USA). Cell cycle analysis data were analyzed using the FlowJo software (version V10, Ashland, OR, USA).

Western Blotting

Total protein lysates were extracted from fresh RB and normal retina tissues for assessing PLK1 expression level. Cultivated Weri-RB1, Y79, and ARPE-19 cell lines were treated with 4 μM ON-01910.Na for 24 h prior to lysate extraction. Extracted protein lysates were assessed with general Western blotting protocol for expressions of PLK1, Cdc25C, cyclin B1, CDK1, ERK1/2, JNK, and p38 MAPK, as well as their phosphorylated isoforms. Selected antibodies are detailed in Table 1.

Animals and Drug Administration

All animal experiments were performed in accordance with the Regulations for the Administration of Affairs Concerning Experimental Animals of P.R. China (2017), and protocols were approved by the Ethics Committee at ZOC. Four to 6-week-old female, Balb/c (nu/nu) immunodeficient mice (Guangdong Medical Laboratory Animal Center, Foshan, China) were kept in a pathogen-free facility with climate control. For intravitreal administration, 2 μl of prediluted 200, 400, 800, and 1600 μM ON-01910.Na, melphalan, or vehicle phosphate-buffered saline (PBS) was injected into the intravitreal cavity, achieving a final injected amount of 0.4, 0.8, 1.6, and 3.2 nmol of delivered drugs per eye, which was equivalent to 0.19, 0.38, 0.76, and 1.52 μg of ON-01910.Na per eye. For retinal function assessment, one intravitreal injection

Table 1. Antibodies Used for Western Blotting

Antibodies	Species	Manufacturer
Anti-PLK1	Rabbit	Cell Signaling Technology
Anti-CDC25C	Rabbit	Proteintech, Wuhan, China
Anti-phospho-CDC25C	Rabbit	ThermoFisher Scientific
Anti-cyclin B1	Rabbit	Proteintech
Anti-phospho-cyclin B1	Rabbit	Cell Signaling Technology
Anti-CDK1	Rabbit	Proteintech
Anti-phospho-CDK1	Rabbit	Abcam
Anti-ERK1/2	Rabbit	Cell Signaling Technology
Anti-phospho-ERK1/2	Rabbit	Cell Signaling Technology
Anti-p38	Rabbit	Cell Signaling Technology
Anti-phospho-p38	Rabbit	Cell Signaling Technology
Anti-JNK	Rabbit	Cell Signaling Technology
Anti-phospho-JNK	Rabbit	Cell Signaling Technology
Anti-GAPDH	Mouse	Absin Bioscience
Anti- -actin	Mouse	Absin Bioscience
Goat-anti-mouse IgG-HRP		Absin Bioscience
Goat-anti-rabbit IgG-HRP		Absin Bioscience

was performed 24 h prior to test. For assessing antitumor effect on orthotopic xenograft, one intravitreal injection was given on day 14 after transplantation. For assessing antitumor effect on subcutaneous xenograft, one peritoneal injection was given on approximately day 14 after transplantation.

Assessment of Retinal Function by Electroretinography

The integrity of retinal function under the effect of intravitreally injected drugs was assessed by scotopic and photopic flash electroretinography (RETI-Port/Scan21 System, Roland-Consult, Brandenburg a. d. Havel, Germany) on both eyes at 24 h after drug administration. The same mouse was used for assessment at certain dosage: one eye was injected with ON-01910.Na, while the contralateral eye was treated with the same dosage of melphalan as the working reference. Following drug administration, all animals were dark adapted for 24 h before electroretinography, and all tests were performed at 19:00 to eliminate potential circadian fluctuations. Two flash intensities (3.0 and 10.0 cds m^{-1}) of scotopic electroretinography were first performed and followed by 10 min of light adaption and photopic electroretinography (3.0 cds m^{-1}). All electroretinography assessments were tested for each animal, respectively, and readings of a- and b-waves were recorded.

Cell-Derived Xenograft (CDX)

For orthotopic (intraocular) transplantation, approximately 2×10^5 freshly prepared resuspension of Weri-RB1 cells were xenografted into the subretinal region, as previously described[25]. Survival and tumorigenic morphological changes were monitored every 24 to 72 h. On day 28, front view images of mouse eyes were taken by a Cannon EOS camera installed on a Clinico BX900 slit-lamp (Haag-Streit, Switzerland), fundoscopic images were taken by Phoenix Micron IV System (Pleasanton, CA, USA), and optical coherence tomography (OCT) was performed with Spectralis HRA/OCT system (Heidelberg, Germany). Mice were sacrificed for enucleation, and eyeballs were fixed and paraffin embedded for subsequent staining analyses. To assess tumor regression in the intraocular xenograft, CDX was established on both eyes of the mice, and treatments were given on day 14 after transplantation. Drugs (ON-01910.Na or melphalan) were delivered intravitreally on only one eye for positivity test, while the other received PBS treatment only and was used as an internal reference for drug efficacy.

For subcutaneous transplantation, approximately 1×10^7 Weri-RB1 cells were injected into the inguinal region of the mice, and palpable tumor appeared approximately 2 weeks after injection. Tumor dimensions were measured every 48 h, and tumor volumes were calculated using the following formula: $0.5 \times a^2b$, where a refers to the smaller dimension of tumor width and b is the dimension perpendicular to a. When the tumors reached ~30 mm^3, tumor-bearing mice were randomized into two groups (six mice per group) and administered with vehicle (drinking water) or ON-01910.Na (intraperitoneal 20 mg/kg). Mice were sacrificed 2 weeks after drug treatment for tumor tissue harvesting.

Paraffin Sections and Staining

All staining for hematoxylin and eosin (H&E), TUNEL (terminal deoxynucleotidyl transferase-mediated deoxyuridine triphosphate nick end labeling), and immunohistochemistry were performed on 5-μm-thick paraffin sections of tissues harvested from mice, with standard protocols finely adjusted with optimized conditions. Histology changes in retinas were examined with H&E staining, evaluated by approximate quantification of nuclei or viable cells in inner nuclear layer (INL) and outer nuclear layer (ONL) per entire section of a retina cut through the optic nerve and optic disc, and three sections were assessed for each eye. TUNEL was stained for identification of cells undergoing apoptosis under the effect of intravitreally administered drugs. Immunohistochemistry was performed for assessing expressions of PLK1 (Cell Signaling Technology, Danvers, MA, USA).

Statistical Analysis

Statistical analyses and calculation of IC_{50} values were performed using GraphPad Prism7 Software (GraphPad Software, San Diego CA, USA). Student's *t*-test and one-way analysis of variance were used for statistical comparison of parametric data between two and multiple groups, respectively. Mann–Whitney and Kruskal–Wallis tests were used for nonparametric comparison between two and multiple groups, respectively. Chi-square test was used for statistical comparison of distribution/proportions. Paired tests were applied where appropriate. Numbers of replicates/samples and p values are stated in each figure legend. All data were expressed as means ± standard error of mean (SEM). Statistical significance was concluded when the p value was less than 0.05, and ns (not significant) denotes $p > 0.05$.

RESULTS

PLK1 Is Aberrantly Upregulated in RB

A total of 331 differentially expressed genes (DEGs) were identified from RNA sequencing of three RB tissues, with reference to three normal retinas (Fig. 1A). DEGs specific to RB were categorized by KEGG pathway enrichment analysis; 10 categories of upregulated DEGs and 2 categories of downregulated DEGs were ranked and among which the cell cycle signaling pathway was the most significantly associated (Fig. 1B). Twenty-five

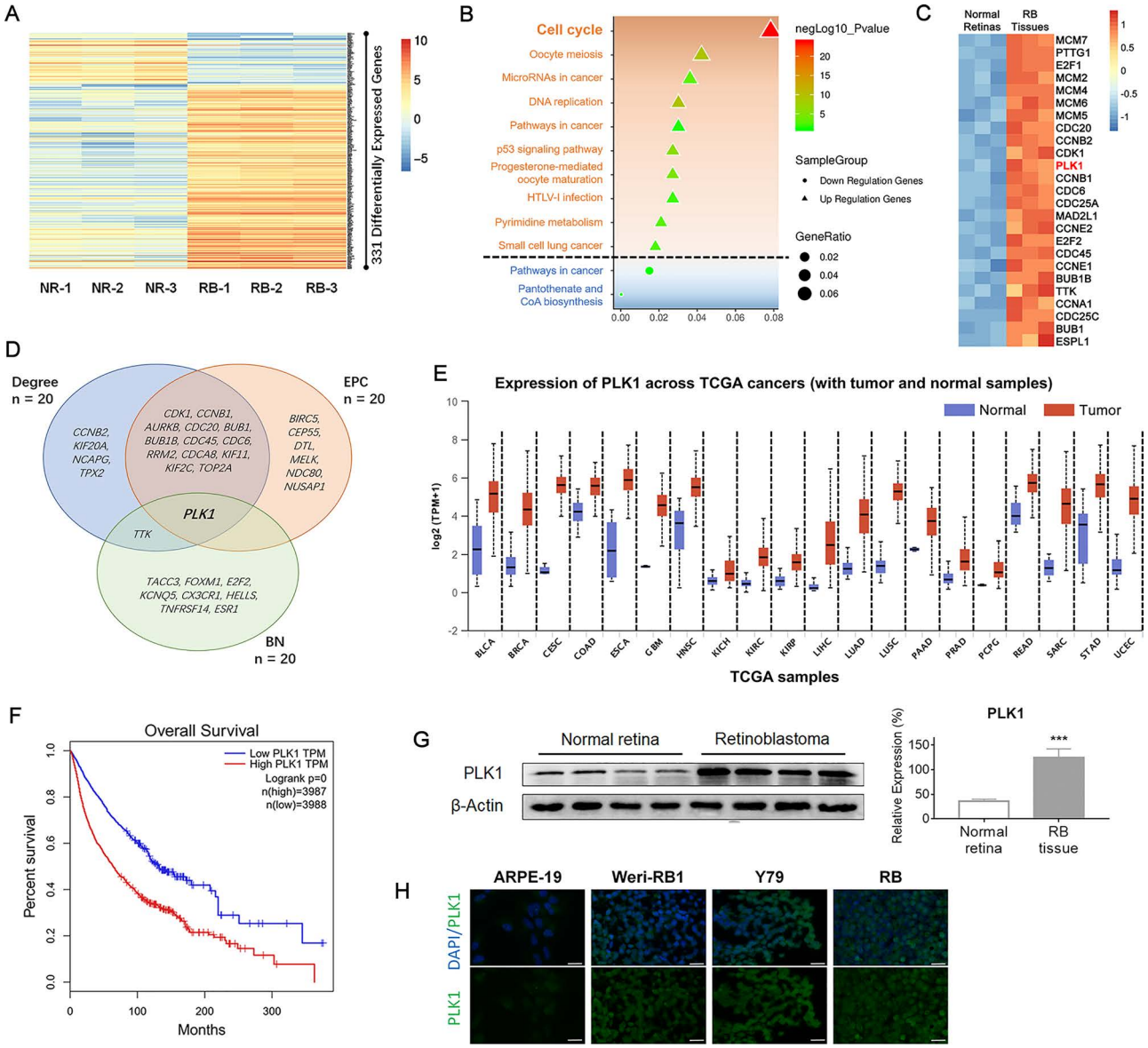

Figure 1. Upregulation of the polo-like kinase 1 (PLK1) pathway in retinoblastomas (RBs). (A) A total of 331 differentially expressed genes (DEGs) were identified from comparative analysis of RNA sequencing data between RB (n = 3) and normal retina tissues (NR, n = 3). (B) Pathway enrichment analysis by Kyoto Encyclopedia of Genes and Genomes demonstrated that the cell cycle pathway was the most prominent among all categories of DEGs. (C) Transcripts of 25 cell cycle pathway-related factors were differentially upregulated in RB (n = 3) tissues in contrast to NR (n = 3). (D) Venn diagram of the top-ranked DEGs identified by three parameters used in topological analysis with the CytoHubba program. (E) *PLK1* expression was found upregulated in 24 types of cancers, according to The Cancer Genome Atlas database, and (F) the Kaplan–Meier survival curve demonstrated that low survival was associated with high level of *PLK1* transcripts (log_rank p = 0). (G) By Western blot, PLK1 protein expression in (left to right, lanes 1–4) RB tissues compared to (left to right, lanes 5–8) NR, and relative expression to -actin (expressed by percentage) was illustrated. (H) Immunofluorescence staining confirms PLK1 expression on RB cells (patient-derived, and Weri-RB1 and Y79 cell lines). Scale bar: 20 μm. Data were calculated from n = 3 replicates and presented as means ± standard error of mean (SEM). EPC, edge percolation component; BN, bottleneck; TPM, transcripts per million. BLCA, bladder urothelial carcinoma; BRCA, breast invasive carcinoma; CESC, cervical squamous cell carcinoma and endocervical adenocarcinoma; COAD, colon adenocarcinoma; ESCA, esophageal carcinoma; GBM, glioblastoma multiforme; HNSC, head and neck squamous cell carcinoma; KICH, kidney chromophobe; KIRC, kidney renal clear cell carcinoma; KIRP, kidney renal papillary cell carcinoma; LIHC, liver hepatocellular carcinoma; LUAD, lung adenocarcinoma; LUSC, lung squamous cell carcinoma; PAAD, pancreatic adenocarcinoma; PCPG, pheochromocytoma and paraganglioma; PRAD, prostate adenocarcinoma; READ, rectum adenocarcinoma; SARC, sarcoma; STAD, stomach adenocarcinoma; UCEC, uterine corpus endometrial carcinoma. Statistical significance at ***$p < 0.001$.

cell cycle-related DEGs were overexpressed specifically in RB tissues, and among these DEGs, several were components involved in, or neighboring of, the PLK1 pathway, such as *AURKA*, *CCNB1*, *CDK1*, *BUB1B*, and *PLK1* itself (Fig. 1C). On the other hand, following analysis of protein interrelationship using the STRING database, 258 hub genes were screened by topological analysis with the CytoHubba program. For each of the three parameters (degree, edge percolation component, and "bottleneck"), the top 20 genes with the greatest values were ranked, and the only one gene that was intersected in three criteria was *PLK1* (Fig. 1D). We next searched *PLK1* expression profile in various types of diseases in the UALCAN data system using the TCGA database; although there were no RB-specific data, *PLK1* was found upregulated in 20 types of tumors or cancers (Fig. 1E). Furthermore, an integrated survival analysis on *PLK1* and the above described 20 cancer types was performed using the GEPIA web application and revealed that lower survival was associated with high *PLK1* expression (Fig. 1F). Despite that transcripts of *PLK1* were differentially upregulated in RB by bioinformatics, it was important to confirm the functional protein expression. Total protein lysates were extracted from four RB and four normal retina tissues for Western blotting of PLK1. The results showed significantly higher PLK1 expression in RB tissues than in normal retinas (Fig. 1G), suggesting that RB tumorigenesis may be associated with aberrant PLK1 expression. Furthermore, PLK1 expressions were confirmed on cultured RB cells, including cell lines Weri-RB1, Y79, and patient-derived RB cells (Fig. 1H), justifying that RB could be a well-suited disease model for targeted therapy against the PLK1 pathway.

ON-01910.Na Results in Tumor-Specific Cytotoxicity in Cultured RB Cells

To validate the targetability of PLK1 in RB cells, we tested cell viability in RB cells (Weri-RB1, Y79, and patient-derived cells) after treatment of ON-01910.Na for PLK1 inhibition. The cytotoxic efficacy was referenced with melphalan, an intravitreal therapy currently used for RB. Tumor specificity was referenced with a nontumor human retinal pigmented epithelial ARPE-19 cell line. A broad-spectrum concentration of ON-01910.Na between 10 nM and 10 μM was initially tested per 10-fold increase, and the viability of RB cells, as measured by CCK-8 MTT assay, was inversely dose dependent (Fig. 2A). The IC_{50} values of ON-01910.Na in ARPE-19, Weri-RB1, Y79, and patient-derived RB cells were 4.97 μM, 1.14 μM, 0.92 μM, and 1.81 nM, respectively, and they were comparable to that of melphalan (11.54 μM, 1.91 μM, 1.52 μM, and 1.93 nM). It is worth noting that the plateau of ARPE-19 viability between 10 nM and 1 μM indicated a possible safety range for nontumor cells. The ARPE-19 viability dropped dramatically between 1 and 10 μM. With more elaborative concentrations, findings revealed that the safety threshold for ARPE-19 was approximately 4 μM ($p < 0.001$) (Fig. 2B). At prolonged incubation of one-time drug treatment, loss of ARPE-19 viability was merely insignificant with treatment of 4 μM or lower, whereas at 4.5 μM, ARPE-19 cell deaths were apparent at 24 h and persistent with longer time of incubation (Fig. 2C). Critical safety concentration of the ON-01910.Na on nontumor ARPE-19 at 4 μM was further confirmed. At this concentration, cell deaths in RB cells were significantly induced compared to ARPE-19. Furthermore, the cell death-inducing capability of ON-01910.Na was outstanding and specified to RB cells only (Fig. 2D). Again, slight variation in sensitivities between RB cell lines and patient-derived cells was noted. In order to investigate cell viability under longer drug exposure times, RB cells were treated with ON-01910.Na for 12, 24, 36, 48, 72, and 96 h (Fig. 2E). The decrease in RB cell viability was most significant within the first 24 h, and cell viability was inversely dependent on the length of exposure time ($r = -0.9216$, $p = 0.0032$ and $r = -0.8944$, $p = 0.0066$, respectively); the ARPE-19 demonstrated increase in cell viability after 48 h of drug treatment. Cell viability of ARPE-19 treated with 4 μM ON-01910.Na for various exposure periods was significant from RB cell lines ($p < 0.001$). Further evidence of apoptotic status was confirmed by flow cytometry, as shown by detection of total apoptotic cells in quadrants Q2 and Q3 (Fig. 2F).

3D cultures have gained increasing interest in cancer studies and drug discovery as they are expected to resemble in vivo cell environments and accommodate better precision in drug discovery. While patient-derived cells were grown into 3D tumor spheroids under a conditioned Matrigel setting, 4 μM ON-01910.Na, melphalan, or vehicle (DMSO) was applied for 24 h. Under direct microscopic observation, cell deaths, as marked by trypan blue dye, were seen in the majority of cells treated with ON-01910.Na and melphalan. Density of trypan blue staining was an indication for the extent of overlaying cell deaths, and it was scaled and labeled with standardized color for subsequent area estimation. For instance, the dark trypan blue staining labeled in red indicates multiple spheroid layers of cell death and suggests in-depth penetration of drug efficacy. It was worth noting that ON-01910.Na was able to penetrate and cause cell deaths in larger tumor spheroids despite that the proportion of drug-induced cell deaths was similar between ON-01910.Na and melphalan (Fig. 2G). For longer drug exposure effect on tumor spheroids, the same concentration of ON-01910.Na (or melphalan) was applied for 48 h. Microscopic observation revealed that cell death, as indicated by trypan blue, was seen in almost all tumor spheroids, and the extent of spheroid layers of cell death was similar between ON-01910.Na and melphalan treatments (Fig. 2H).

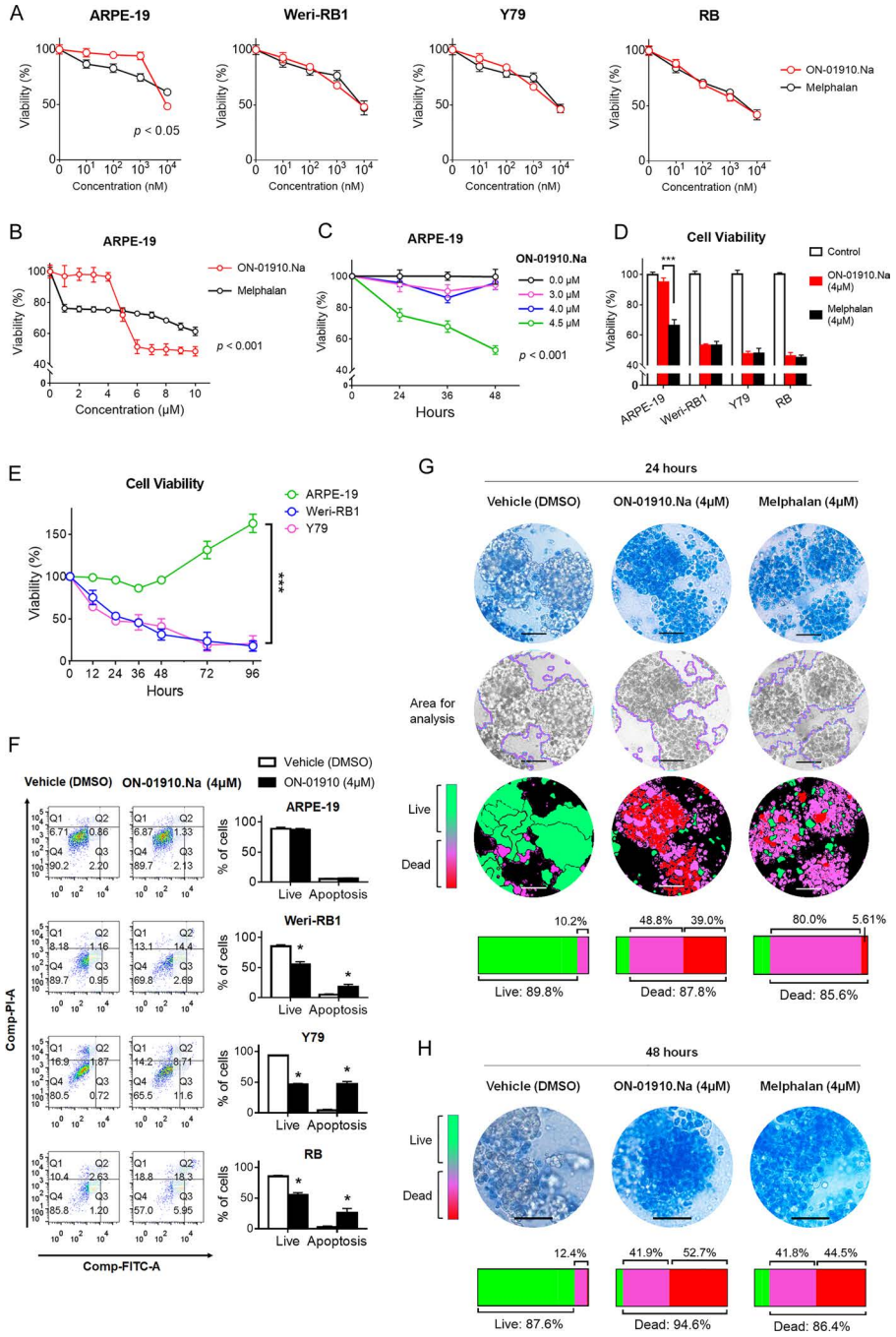

Figure 2. In vitro cytotoxicity of ON-01910.Na. (A) At the concentration range between 10 and 10 μM, ON-01910.Na was dose-dependently cytotoxic to Weri-RB1, Y79, and patient-derived RB cells, and the cytotoxicity was comparable to that of melphalan. (B) ON-01910.Na-induced cytotoxicity on ARPE-19. (C) Cytotoxicity of 3.0, 4.0, and 4.5 μM ON-01910.Na on ARPE-19 for treatment from 24 to 48 h. (D) Cytotoxicity of 4 μM ON-01910.Na or melphalan on ARPE-19, Weri-RB1, Y79, and RB. (E) Cell viability of ARPE-19, Weri-RB1, and Y79 treated with 4 μM ON-01910.Na for various drug exposure periods: 12, 24, 36, 48, 72, and 96 h. (F) Flow cytometry for apoptosis showed proportion of living cells (Q4) and cell deaths (Q2 and Q3) in cultured ARPE-19, Weri-RB1, Y79, and RB with or without treatment of 4 μM ON-01910.Na: cell deaths was detected by increased fluorescein isothiocyanate (FITC) signal (label of annexin V). (G) Representative microscopic images of cell death in three-dimensional spherical culture induced by 4 μM ON-01910.Na for 24 h; visualization was aided by addition of typan blue dye. Density of staining was scaled by three colors: green (live cells), magenta (apoptotic cells), and red (apoptotic cells in multiple spheroidal layers). Proportion of cell death was calculated by estimated area coded magenta and red. (H) Representative microscopic images of three-dimensional spherical culture treated with 4 μM ON-01910.Na for 48 h. Scaling bar: 50 μm. For all data points, data were calculated from at least $n = 3$ replicates and presented as means ± SEM. Statistical significance at $^{*}p < 0.01$, $^{***}p < 0.001$.

Inhibition of PLK1 Pathway Leads to Cell Cycle Arrest in RB Cells

Here we addressed changes in protein levels of various PLK1 pathway factors in cultured RB cells. A schematic diagram was illustrated for an activated PLK1 signaling pathway (Fig. 3A). The pathway involves PLK1-facilitated phosphorylation of Cdc25C, which in turn dephosphorylates CDK1, leading to phosphorylation of cyclin B1, and the CDK1/cyclin B1 dimer is subsequently activated and relocates into the nucleus for cell cycle progression.

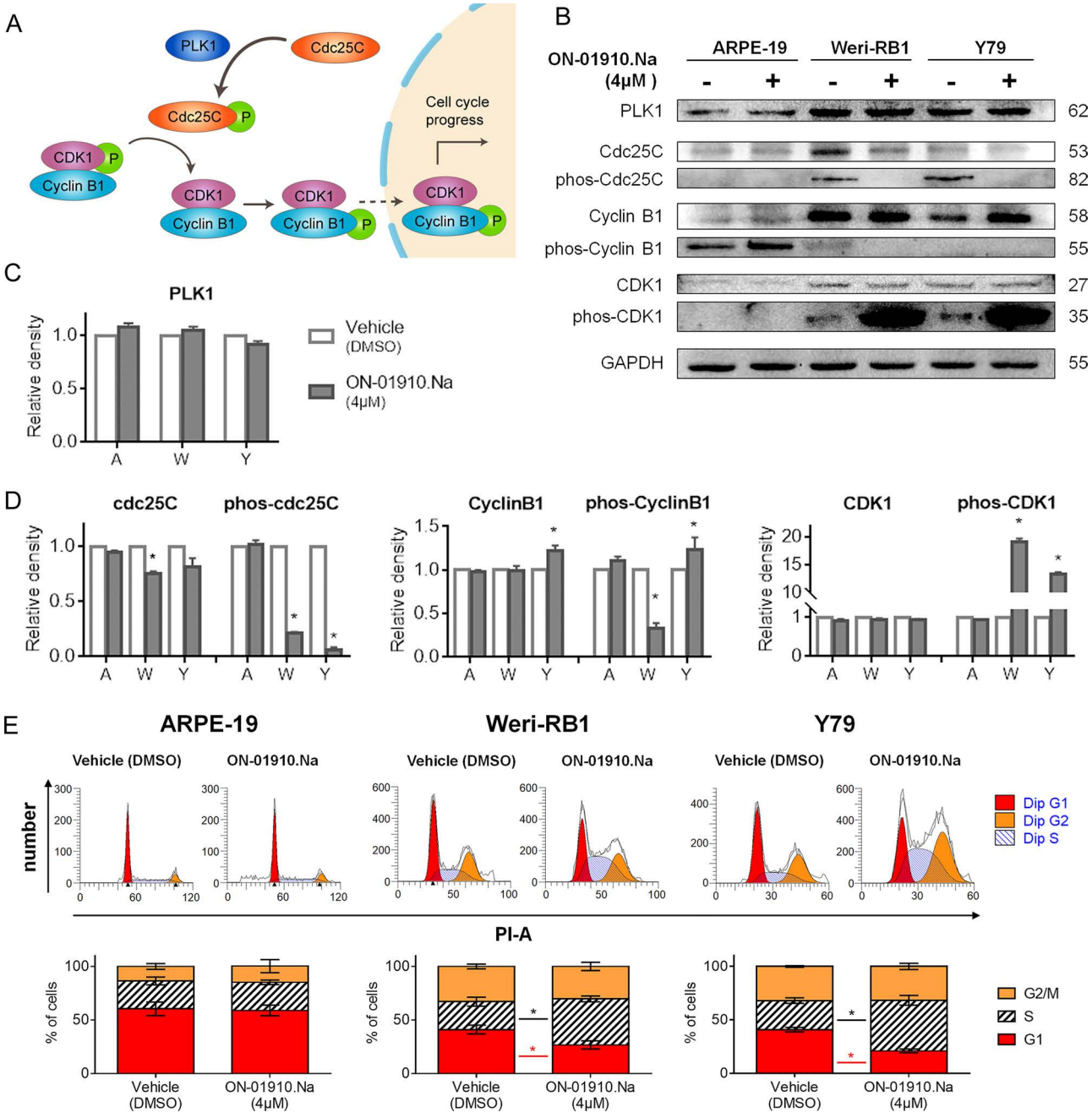

Figure 3. Inhibition of PLK1 pathway and cell cycle arrest. (A) A brief illustration of an activated PLK1 pathway: PLK1 activates Cdc25C and relocates activated CDK1/cyclin B1 complex into the nucleus in order to enhance cell cycle progress. (B) Western blot and semiquantification of expression level changes in (C) PLK1, (D) Cdc25C, cyclin B1, and CDK1 as well as their phosphorylated forms (labeled as "phos"), with and without treatment of 4 μM ON-01910.Na in ARPE-19, Weri-RB1, and Y79, respectively. (E) Flow cytometry for cell cycle analysis on ARPE-19, Weri-RB1, and Y79. For all data points, data were calculated from $n = 3$ replicates and presented as means ±SEM. A, ARPE-19; W, Weri-RB1; and Y, Y79. Statistical significance at $^*p < 0.05$.

Following treatment of 4 μM ON-01910.Na or vehicle (DMSO) on cultured cells, total lysates were extracted and subjected to immunoblotting for analyses of downstream factor protein levels (Fig. 3B–D). In ARPE-19, while PLK1 expression was mild, none of the Cdc25C, CDK1, cyclin B1, and their phosphorylated forms demonstrated significant protein level changes, suggesting its persistence to PLK1 inhibition. In contrast, for Weri-RB1 or Y79, suppression of Cdc25C phosphorylation and accumulation of phosphorylated CDK1 suggested that the RB cells were sensitive to drug application and the PLK1 pathway was successfully inactivated.

Inactive cyclin B1/CDK1 protein complex pauses the entry into mitosis, which leads to cell cycle arrest at the G_2/M phase. Flow cytometry for cell cycle analysis revealed that in the RB cell lines, there was conspicuous decrease in cell proportion at the G_1 phase, accumulation of cell population at the S phase, and increase in the ratio of the G_2/M to G_0/G_1 cell population, together suggesting a possible shift and arrest of cell cycle at the G_2/M phase under the effect of ON-01910.Na (Fig. 3E). Nontumor reference ARPE-19 was merely affected and neither were levels of expression or cell cycle changes.

Cellular Response Induced by PLK1 Inhibition Triggers MAPK Signaling

Our in vitro findings suggested that at concentrations below 4 μM of ON-01910.Na, PLK1 inhibition was highly specific to RB cells. We therefore performed transcriptomic analysis to study cellular response under drug effect. Clustering analysis showed that ARPE-19 did not change significantly between treatments of ON-01910.Na and vehicle; posttreatment transcriptomic alteration in both Weri-RB1 and Y79 was significant (Fig. 4A). There were more DEGs identified in Weri-RB1 and Y79 (2,726 and 2,178 DEGs, respectively) compared to ARPE-19 (639 DEGs) (Fig. 4B). KEGG pathway enrichment analysis (false discovery rate, <0.05) revealed that MAPK signaling cascade was enriched with greatest DEG counts (n = 66) in Weri-RB1 and Y79 (Fig. 4C). In contrast, with the same cutoff, there was no category of DEGs identified in ARPE-19. Among the 66 DEGs of MAPK category, 27 DEGs were upregulated in both Weri-RB1 and Y79 (Fig. 4D).

The MAPK signaling cascade includes various pathways led by different MAP kinases, such as p38 MAPK, JNK/stress-activated protein kinase (SAPK), and ERK1/2, and are responsible for a wide range of cellular processes. Activation of p38 and JNK is involved in cell death and stress responses, while ERK1/2 is usually associated with cell proliferation. With treatment of PLK1 inhibitor, immunoblotting revealed that total and phosphorylated p38 MAPK and JNK were upregulated in RB cells, suggesting these pathways may be activated toward cell death following PLK1 inhibition (Fig. 4E and F). In contrast, ERK1/2 expression and phosphorylation were decreased, implying that the ERK1/2 pathway may be suppressed as cell proliferation was inhibited with PLK1 inhibition.

To further elucidate our findings on the MAPK mechanism, we applied inhibitors of p38 MAPK (BMS-582949 HCl), JNK (SP600125), and ERK1/2 (SCH772984) to the Y79 cell line, which showed higher sensitivity to PLK1 inhibition. Cell viabilities were assessed in response to 24-h cotreatment for ON-01910.Na and MAPK inhibitors. Inhibition of p38 MAPK and JNK resulted in a dose-dependent increase in cell viability in Y79, indicating a survival rescue from cytotoxicity induced by PLK1 inhibition (Fig. 4G). Conversely, increased cell death was observed in cells treated with 10 μM ERK1/2 inhibitor. Taken together, activation of p38 MAPK and JNK is triggered by ON-01910.Na, and these pathways are preceding processes to apoptosis.

Intravitreal ON-01910.Na Improves Ocular Survival by Preserving Retinal Functions and Structures

Before antitumor efficacy could be tested, assessment for translational safety in animals was essential, and for "targeted therapy," we aimed to preserve eyesight. Survival of eyesight was evaluated by the integrity of the retinal function, which was assessed by electroretinography, where ON-01910.Na, melphalan, or vehicle (PBS) was intravitreally injected into the Balb/c nude mice at various doses 24 h prior to assessment. Representing data from scotopic 3.0 electroretinography demonstrated that the amplitudes of a- and b-waves were compared among eyes treated with vehicle, ON-01910.Na, and melphalan of various doses (0.4, 0.8, 1.6, and 3.2 nmol per eye, respectively) (Fig. 5). The potential effect of vehicle PBS was excluded by comparison with nontreated contralateral eye (Fig. 5A). To eliminate conceivable physiological variances among individual mice, the effect of ON-01910.Na on the retina was compared with contralaterally treated melphalan (Fig. 5B). Retinal function was maintained at 0.4 and 0.8 nmol intravitreal ON.01910.Na until it reached 1.6 nmol and higher. During scotopic electroretinography, the response of photoreceptors, as measured by a-wave, was relatively stable with increased ON-01910.Na (Fig. 5C); the response of Müller cells and bipolar cells, as measured by b-wave, was more susceptible to the effect of the drugs (Fig. 5D). Our electroretinography findings suggested that under a safety dosage (i.e., 0.8 nmol per mice eye), ON-01910.Na does not induce ocular function impairment, and the retinal function was well preserved.

Structural changes of the retina were evaluated by cross-sectional histology of eyes enucleated 24 h after local drug administration. H&E staining revealed that no

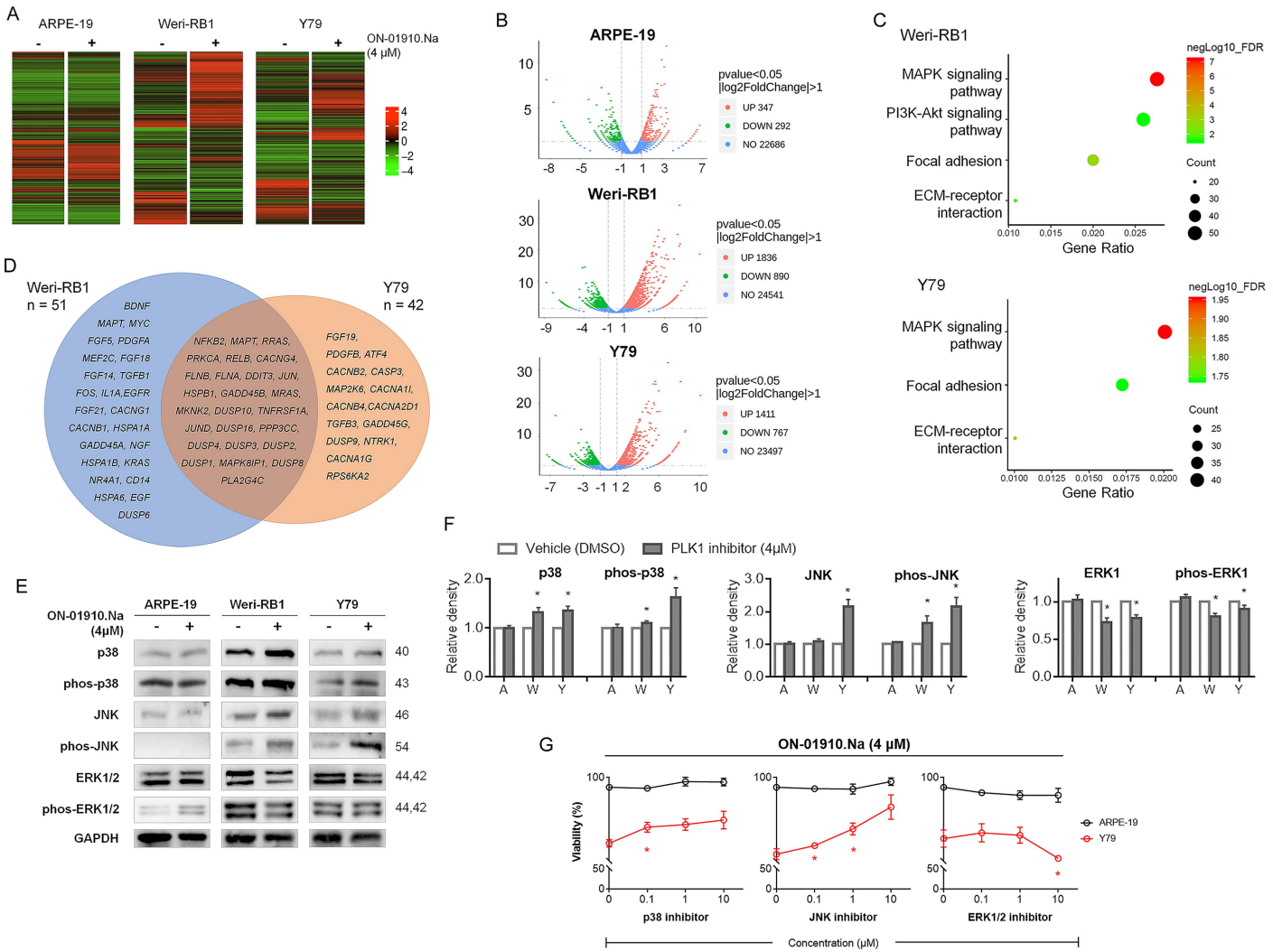

Figure 4. Transcriptome analysis on cells following treatment with ON-01910.Na. (A) Clustering analysis heat map for comparison of transcriptome expression patterns between treatments of vehicle (−, DMSO) and ON-01910.Na (+, 4 μM for 12 h). Expression volume of each gene was log2-transformed fragments per kilobase of exon per million fragments mapped (FPKM). (B) Volcano plot of number of DEGs identified in (top to bottom) ARPE-19, Weri-RB1, and Y79 after treatment with ON-01910.Na. (C) Kyoto Encyclopedia of Genes and Genomes pathway enrichment analysis, cutoff at false discovery rate (FDR) <0.05. (D) Venn plot of MAPK signaling pathway-relevant DEGs intersected between Weri-RB1 and Y79. Gene names are listed in the diagram. (E) Western blot and (F) semiquantification of expression level changes in extracellular signal-regulated kinase 1/2 (ERK1/2), p38 mitogen-activated protein kinase (MAPK), and c-Jun N-terminal kinase (JNK) and their phosphorylated expressions following ON-01910.Na treatment. (G) Cell viability of ARPE-19 and Y79 under 24 h cotreatment of 4 μM ON-01910.Na with inhibitors of (left to right) ERK1/2, p38 MAPK, and JNK for 24 h. For all data points, data were calculated from $n = 3$ replicates and presented as means ± SEM. A, ARPE-19; W, Weri-RB1; and Y, Y79. Statistical significance at $^*p < 0.05$.

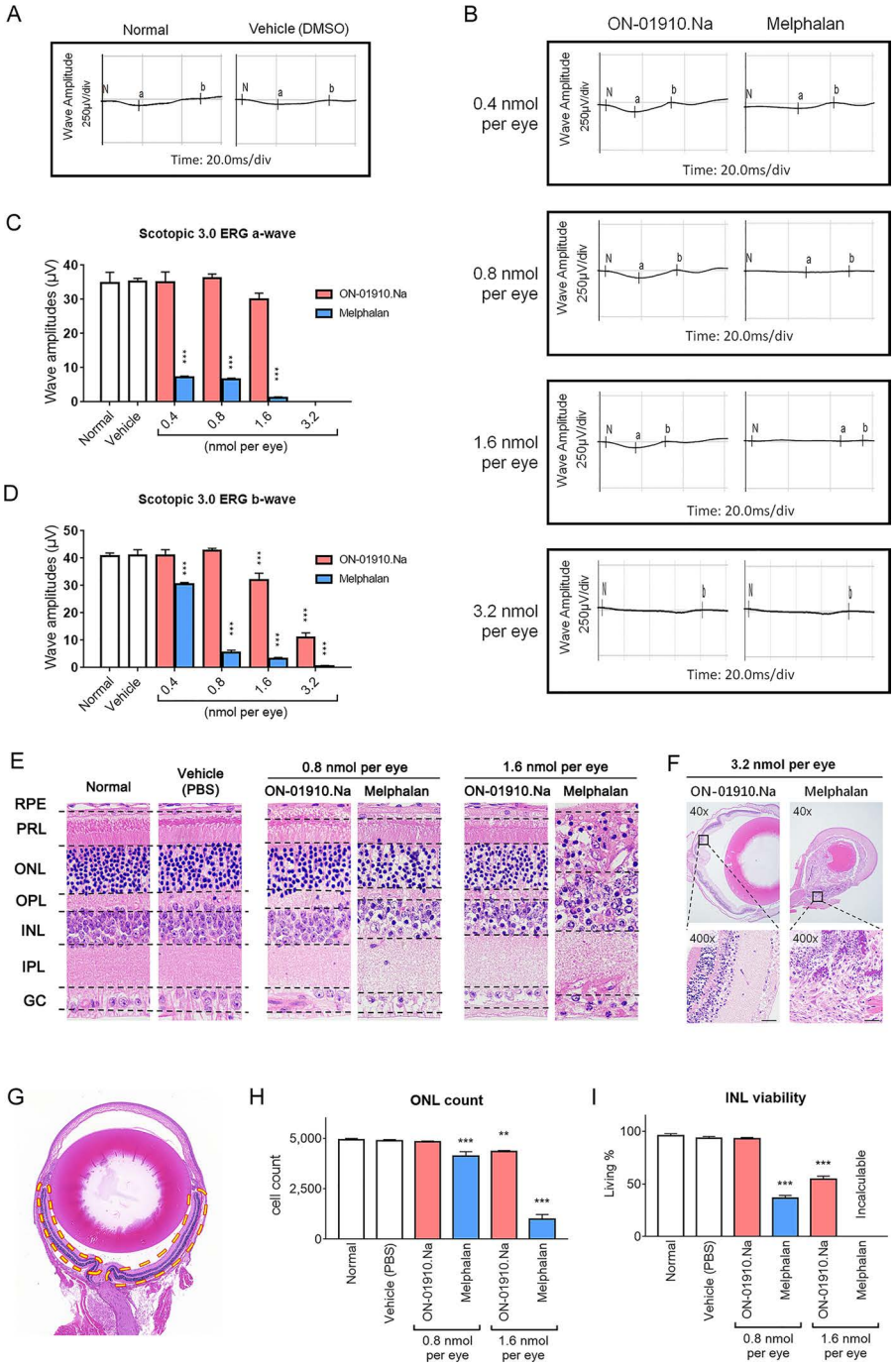

Figure 5. Retinal function and structural assessment following treatment of ON-01910.Na. Scotopic 3.0 cds m^{-1} electroretinography for evaluation of retinal function. (A) Representative electroretinographic charts for normal mice eyes and intravitreal treatments with vehicle (PBS) and (B) at various doses of ON-01910.Na and melphalan (0.4, 0.8, 1.6, and 3.2 nmol per mice eye). (C, D) Electroretinographic amplitudes of responsive a- and b-waves, respectively. (E) Representative histology of retinas, treated with vehicle, ON-01910.Na (0.8 and 1.6 nmol per eye), or melphalan (0.8 and 1.6 nmol per eye) (magnification: ×400). (F) Representative image of ocular toxicity in mouse eyes treated with 3.2 nmol of (left) ON-01910.Na and (right) melphalan. Scale bar: 50 μm. (G) Cross section of a mouse enucleation cut through the optic nerve: cell viability was approximately quantified per whole section of retina, as labeled in looped region. (H) Outer nuclear layer (ONL) was quantified by counting of nuclei. (I) Inner nuclear layer (INL) was estimated by approximate percentage of nonnecrotic region. Results were calculated from $n = 3$ biological replicates and presented as means ± SEM (**$p < 0.01$, ***$p < 0.001$). Electroretinography outputs: x axis, time, 20.0 ms per grid; y axis, wave amplitude, 250 μV per grid. RPE, retinal pigment epithelium; PRL, photoreceptor layer; OPL, outer plexiform layer; IPL, inner plexiform layer; GC, ganglion cells. ON-01910.Na was used for PLK1 inhibition.

significant alterations in the retina were found in those animals treated with intravitreal 0.8 nmol ON-01910.Na (Fig. 5E). For those eyes treated with 1.6 and 3.2 nmol ON-01910.Na, disruption in retinal structures was observed, showing atrophy and post-cell death gaps in the INL, as well as pale, edema-like thickening of inner plexiform layer (IPL) (Fig. 5E and F). Cell viabilities were evaluated under microscopy observation by quantifying the approximate numbers and proportion of normal nuclei per whole section of central retina for ONL and INL, respectively (Fig. 5G). Compared to normal or vehicle-treated eyes, changes in ONL nuclei count and INL live nuclei proportion were negligible in 0.8 nmol ON-01910.Na-treated mice eyes; however, they were significant in melphalan-treated eyes ($p < 0.001$) (Fig. 5H and I). Our findings were concordant to functional electroretinography, where structural integrity was preferred with ON-01910.Na than with the same dose of melphalan, and retinal layers were well preserved at a dosage of 0.8 nmol per mice eye. Furthermore, at high dose of administration, cells in the INL/IPL, demonstrated by b-waves, were more prone to ON-01910.Na-induced damage.

Intravitreal ON-01910.Na Shows Good Antitumor Effect on Subretinal Tumor Xenograft

First, we addressed whether xenograft tumorigenicity could be inhibited by ON-01910.Na, where it takes effort for small molecules to reach subretinal region and exert cytotoxic effect by penetrating through the retina tissue. Intravitreal ON-01910.Na was immediately administered following Weri-RB1 xenograft, and the dosage was limited to in vivo safety for local retinal tissues (i.e., 0.8 nmol per mouse eye), as above described. In contrast to vehicle PBS treatment ($n = 10$ eyes, 70% developed tumors), xenograft tumorigenesis was successfully suppressed by administered ON-01910.Na or melphalan ($n = 8$ eyes for both groups, zero tumors) (Fig. 6A). Representative images of front view, fundoscopy, and OCT of xenograft mouse eyes were taken on day 14 (Fig. 6B–D). Suspicious retinal detachments were apparent with vehicle-treated eyes, and OCT image indicates that there may be neoplastic mass underlying the subretinal xenograft site. Histopathology observation by H&E staining confirmed development of xenograft tumor in eyes treated with vehicle, while there were no tumors developed in eyes treated with ON-01910.Na or melphalan (Fig. 6E). Histological structure of retinal layers was maintained for ON-01910.Na-treated eyes, suggesting that penetration of ON-01910.Na and inhibition of subretinal tumorigenesis were efficient without affecting the normal retina.

Next, an intraocular tumor-regressing model was established by intravitreally injecting 0.4 nmol ON-01910.Na (PBS in contralateral eye) on day 14 following initial tumor xenograft ($n = 8$ mice, bilateral CDX). Immunohistochemistry of PLK1 confirmed positivity on xenograft tumors (Fig. 6F). Tumor tissue regression was shown in histopathological staining and confirmed with positive TUNEL staining, revealing that apoptotic cell deaths in xenograft RB were apparent in subretinal or vitreous regions (Fig. 6G and H).

Further evidence of ON-01910.Na antitumor activity was demonstrated in subcutaneous xenograft. We found that tumor mass was significantly reduced in the mice injected with ON-01910.Na for 14 days ($n = 6$) compared with the vehicle-treated group ($n = 6$) (Fig. 6I). The H&E staining confirmed histopathology for xenograft tumor and demonstrated a large area of necrotizing tumor tissue with ON-01910.Na treatment (Fig. 6J). More importantly, no significant histology changes in kidney and liver tissues were observed (Fig. 6K).

DISCUSSION

Initiation of tumor development requires consistently inactivated tumor suppressors, which are usually regulators of the cell cycle and cell proliferation processes. Abnormal cell cycle progression is often associated with aberrant protein kinases, such as PLK1, which is overexpressed in a wide range of cancer types, and has been identified as an oncogene[14,27].

PLK1 is an essential regulator of the DNA damage checkpoint and the DNA repair process[28], and it is responsible for mitotic entry during cell cycle progress[29]. PLK1 expression is found in highly proliferative tissues, and many studies have reported that PLK1 overexpression is associated with the tumor grading, metastasis and patients' prognosis, and drug resistance in cancer therapies of various mechanisms[14,16,27,29]. Like other protein kinases, PLK1 is considered as a target for cancer drug development[10,30]. To date, only few studies addressed the relevance of PLK1 in RB. Our bioinformatic findings showed that transcripts of *PLK1* and neighboring factors such as *AURKA*, *BUB1*, *CDK1*, *CDC25C*, and *CCNB1* were elevated in RB tissues compared to normal retinas, suggesting possible linkage between the PLK1 pathway and tumorigenesis, and the feasibility of targeted therapy in RB.

As a potential target for anticancer therapy, inhibition of the PLK1 pathway has been studied in several cancer cell lines[31–33]. The PLK1 pathway includes various factors such as Cdc25C, cyclin B1, and CDK1. The cyclin B/CDK1 complex is activated by phosphorylation of cyclin B1 and dephosphorylation of CDK1, which in turn leads to nuclear translocation for mitotic entry. Similar to previous studies, with PLK1 inhibition, our results demonstrated accumulation of inactivated cyclin B1 and phosphorylated CDK1[20,34]. Inactivated cyclin B/CDK1 dimer results in failure of nuclear translocation for mitosis, and cell cycle arrest at the G_2 phase is a result of PLK1

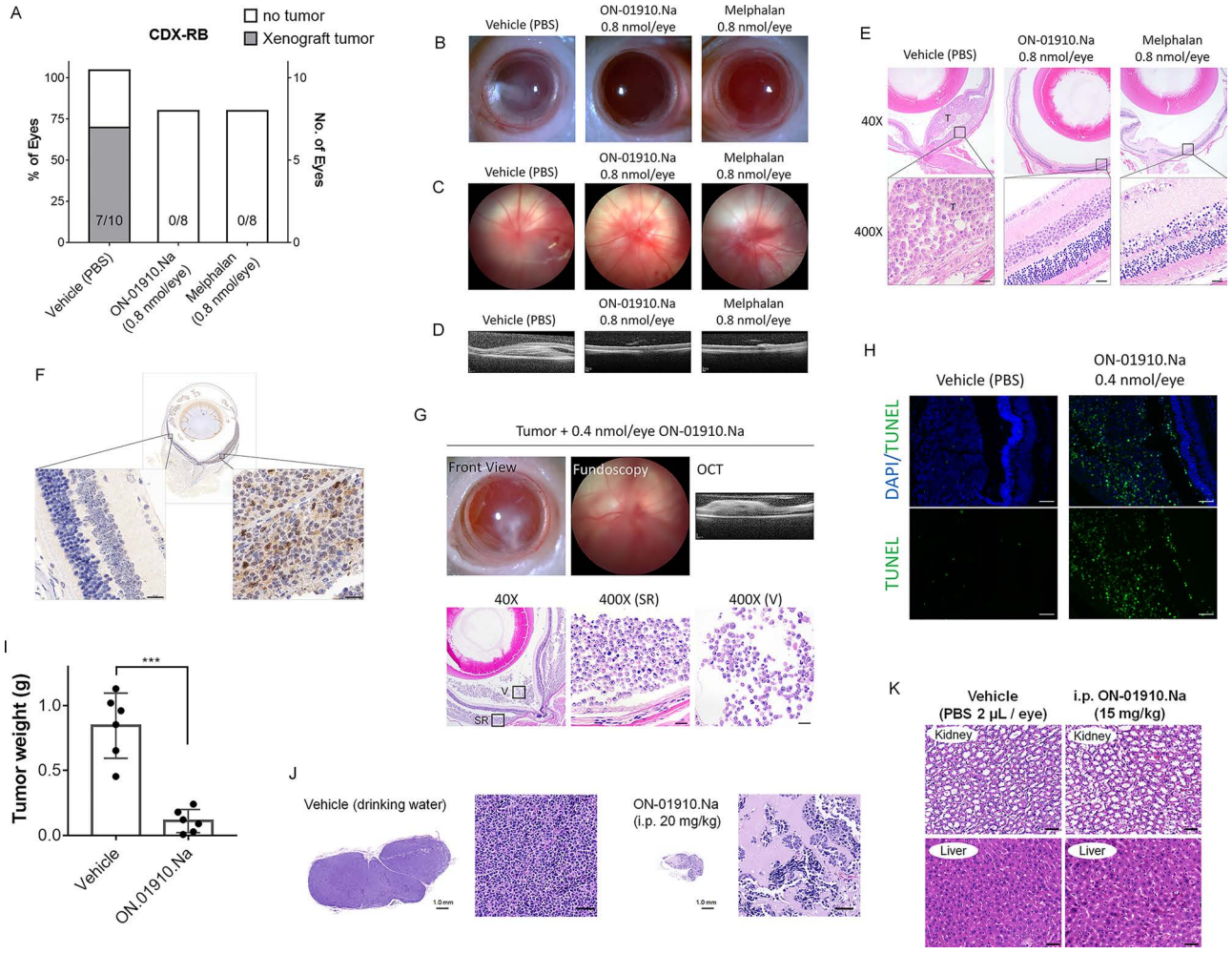

Figure 6. Xenograft RB in Balb/c nude mice. (A) Number of xenograft tumors by subretinal implantation of 2×10^5 Weri-RB1, with intravitreally coadministered vehicle (n = 10 eyes), 0.8 nmol ON-01910.Na (n = 8 eyes), or melphalan (n = 8 eyes) per eye. (B) Representative image of frontal views of eyes on 28 days postxenograft; cloudiness was suspicious of intraocular neoplasms. (C) Representative fundoscopic images and (D) optical coherence tomography (OCT) of retinas showing possible retinal detachment due to subretinal xenograft tumor formation in vehicle-treated mice. (E) Hematoxylin and eosin (H&E) of enucleated eyes revealing xenograft tumors in vehicle-treated eyes and failure to induce tumor development in ON-01910.Na or melphalan-treated eyes. Scale bar: 20 µm. (F) Immunohistochemical staining of PLK1 on a mouse xenograft eye. The retina was negative for PLK1 (bottom left), meanwhile the xenograft RB was positive for PLK1 (bottom right). Scale bar: 20 µm. (G) Tumor regression model was established by intravitreal 0.4 nmol ON-01910.Na treatment on day 14 postxenograft. Representative frontal view, fundoscopy, and OCT were acquired. Histopathology by H&E showed tumor cell deaths in both subretinal (SR) and vitreous (V) seeding. Scale bar: 20 µm. (H) TUNEL (terminal deoxynucleotidyl transferase-mediated deoxyuridine triphosphate nick end labeling) staining on 0.4 nmol ON-01910.Na-treated xenograft: more cell deaths than in phosphate-buffered saline (PBS)-treated RB, and retina was well preserved. Scale bar: 50 µm. (I) Weights of subcutaneous tumors from mice receiving vehicle (drinking water) or intraperitoneal ON-01910.Na (20 mg/kg) treatments. (J) Representative image of H&E staining on xenograft tumor tissues. (K) Representative image of H&E staining on kidneys and livers in mice with subcutaneous xenograft and received vehicle (drinking water) or intraperitoneal (i.p.) ON-01910.Na treatment. Scale bar: 50 µm. Results were calculated from n = 6 biological replicates and presented as means ± SEM (***$p < 0.001$).

inhibition[16]. In agreement with previous studies[33,35], we found accumulation of cell population at the G_2 phase.

Molecular mechanisms following PLK1 inhibition were further investigated with bioinformatic and pathway analyses, and our results suggested that the MAPK signaling cascades were activated in tumor cells. The MAPK cascades, including p38 MAPK, JNK/SAPK, and ERK1/2 pathways, are involved in the regulation of a wide range of cellular processes such as cell proliferation, survival, and apoptosis[36–38]. Both p38 MAPK and JNK/SAPK may exhibit an apoptotic-driving function[39,40], and concordantly, we found elevated levels of these MAPKs after PLK1 inhibition. Also, inhibition of p38 and JNK on tumor cells demonstrated survival rescue

from ON-01910.Na treatment. With the same small-molecule inhibitor ON-01910.Na used, Chapman et al.[41] reported that it induced oxidative stress in leukemic cells and activated JNK/SAPK response, which was similarly demonstrated in our study. The ERK1/2 pathway is commonly associated with cell growth[42] and is thought to be associated with the development of cancers. A previous study demonstrated suppressed proliferation in non-small cell lung cancer cells by PLK1 inhibition[35], whereas our results showed decreased ERK1/2 expression, indicating that PLK1 inhibition may have overcome the survival of RB cells. The MAPK cascade is complex and may exhibit various functions and responses for cellular processes; hence, the in-depth understanding of MAPK signaling remains to be further investigated.

PLK1 pathway inactivation, cell cycle arrest, mitotic catastrophe, and MAPK cascade response to stress are preceding events to RB cell death after treatment of ON-01910.Na. The in vitro cytotoxicity of ON-01910.Na has been tested in more than 100 cell lines[31,33,43]. We demonstrated that the viability of RB cells treated with ON-01910.Na was dose and time dependent. More importantly, cytotoxicity of ON-01910.Na has been found tumor selective in chronic lymphocytic leukemia[41], and concordantly, we found it specifically efficient with RB cells. As for nontumor control, due to the lack of availability and reliable retinal cell lines[44], ARPE-19 is yet the most suitable control cell line representing RB-originating tissue, and its viability was well maintained within a safety range of concentration, and the IC_{50} value was much higher than that of the RB cells.

To better resemble in vivo cell environments and accommodate better precision in drug discovery, we also investigated the cytotoxicity in 3D tumor spheroids of patient-derived RB cells with ON-01910.Na. In the 3D model, overlaying of cell deaths in spheroidal layers was evaluated by density of trypan blue staining, which was labeled in three colors for live (green) and dead cells (magenta to red, with increasing overlay of cell deaths). Proportion of drug-induced cell death was estimated using the area coded with magenta and red. In 3D culture, we found that cell deaths in deeper layers of larger tumor spheroids were induced by ON-01910.Na in 24 h; yet in 48 h of treatment, ON-01910.Na and melphalan were equally cytotoxic to the RB spheres as the proportion of deeper layer cell death was not significantly different.

RB is an intraocular malignancy. By using the RB model, we were the first to locally apply ON-01910.Na to intraocular xenograft. Previous studies have shown inhibition to tumor growths in in vivo xenograft models with intraperitoneal treatment of ON-01910.Na[31,45]. Our findings demonstrated complete suppression of intraocular xenograft tumorigenesis in mice by local administration. In addition, we demonstrated effective tumor regressing effect on established tumors of both intraocular and subcutaneous xenografts with intravitreal and intraperitoneal ON-01910.Na injections.

Goals of therapy for RB consist of salvage of life, globe, and vision, and fortunately, treatment of RB has improved significantly in recent decades with survival rates at approximately 90%[46,47]. In the past, carboplatin, vincristine, and etoposides were commonly used as conventional systemic chemotherapeutic agents and/or combined with focal therapy; however, intravenous chemotherapy can lead to serious adverse toxic response including myelosuppression and infection[48,49]. In order to overcome the constraint of blood–retinal barrier and difficulty of achieving sufficient drug exposure in the eye[50], local delivery by intra-arterial chemotherapy or intravitreal injection are methods that localize treatment exposure to the lesion and minimize potential systemic effects[51,52]. Melphalan is currently known the most efficient and commonly used drug in these local chemotherapeutic routes[47,51]. In this study, we aimed to investigate antitumor efficacy of ON-01910.Na by local administration; therefore, we used melphalan as a positive control drug as a reference.

For many sickened children, failure to preserve vision is a negating factor for their quality of life. In our study, mice eyes treated with melphalan demonstrated severe ophthalmic damages such as ocular atrophy and retina fragmentation. ON-01910.Na is antitumor effective at both cellular and animal levels. It is important that "targeted" therapeutic drugs are "tumor specific" to at least minimize damages and avoid functional impairments in collateral nontumor retinal structures.

There are about 10 PLK1-selective compounds currently undergoing research and trial phases, and ON-01910.Na/rigosertib has been studied in clinical trials of various phases. Rigosertib demonstrated good tolerance in higher-risk myelodysplastic syndrome patients failing hypomethylating agents in phase I/II clinical trials[53], and appeared advantageous in selected groups in randomized phase III trial in comparison with best-supportive care[54]. Rigosertib has also entered clinical trials for other malignancies such as metastatic pancreatic cancer (phase II/III)[55], advanced cancers (phase I)[19], and solid tumors (phase I)[56]. ON-01910.Na was chosen in this study for its readiness to be applied clinically. In this preclinical study, we were able to demonstrate efficient antitumor activity in intraocular xenograft without systemic toxicity. More importantly, we demonstrated preferable safety of ON-01910.Na on mouse retinas, suggesting manageable clinical risks in trials on RB patients. Also, even with intraperitoneal administration of ON-01910.Na, histology of mouse kidneys and livers was not adversely affected. Local delivery of ON-01910.Na has overcome the problem of blood–retinal barrier, reduces

drug metabolism, and contains the drug efficacy in the confined intraocular cavity. Moreover, ON-01910.Na has shown to be synergistically effective to raise sensitivity in response to radiotherapy and other chemotherapy agents[57]. To the best of our knowledge, there has been no reports on local administration of ON-01910.Na, either alone or in combination, and ocular-associated complications in human subjects.

The major limitation in our study was the difficulty to accurately translate the dosage used in in vivo mice model to clinical application. Although our results demonstrated effective antitumor activity of ON-01910.Na, the limited size of tumors in the mouse eye does not promise precise estimation of the efficacy in human translation. Therapeutic relevance of local application of ON-01910.Na on human intraocular tumors needs to be investigated.

In summary, this was the first study that investigated the PLK1 targetability in RB, specifically with local administration of ON-01910.Na. This study is supportive for prospective investigation on the potency of clinical translation of targeting PLK1 in RB for aiding eyesight preservation. Importantly, our study provides a novel strategy of local application of ON-01910.Na for not only RB but also other PLK1-aberrant tumors.

ACKNOWLEDGMENTS: The work was financially supported by the High-level Hospital Construction Project (303010406) and Natural Science Foundation of Guangdong Province in China (General Program No. 2019A1515010361). Doctors Huan Ma and Cong Nie contributed equally to this work. R.L., H.M., C.N., and Y.G. conceptualized the study; C.N. and Y.G. performed bioinformatics analyses; Y.G. and P.Y. collected human retinoblastoma samples; H.M., C.N., Y.X., Q.S., and Z.T. carried out in vitro experiments; H.M., C.N., Y.C., J.L., and Y.X. together carried out animal experiments; C.N., S.A., and H.M. collected experimental data; C.N. and H.M. performed experimental data analysis; H.M., R.L., Y.M., H.Y., and N.C. wrote the article. All authors read and approved the final version of the article. The authors declare no conflicts of interest.

REFERENCES

1. Knudson AG, Jr. Mutation and cancer: Statistical study of retinoblastoma. Proc Natl Acad Sci USA 1971;68:820–3.
2. Hamid AA, Gray KP, Shaw G, MacConaill LE, Evan C, Bernard B, Loda M, Corcoran NM, Van Allen EM, Choudhury AD, Sweeney CJ. Compound genomic alterations of TP53, PTEN, and RB1 tumor suppressors in localized and metastatic prostate cancer. Eur Urol. 2019;76:89–97.
3. Chen L, Liu S, Tao Y. Regulating tumor suppressor genes: Post-translational modifications. Signal Transduct Target Ther. 2020;5:90.
4. Cavenee WK, Hansen MF, Nordenskjold M, Kock E, Maumenee I, Squire JA, Phillips RA, Gallie BL. Genetic origin of mutations predisposing to retinoblastoma. Science 1985;228:501–3.
5. Lee WH, Shew JY, Hong FD, Sery TW, Donoso LA, Young LJ, Bookstein R, Lee EY. The retinoblastoma susceptibility gene encodes a nuclear phosphoprotein associated with DNA binding activity. Nature 1987;329:642–5.
6. Chen HZ, Tsai SY, Leone G. Emerging roles of E2Fs in cancer: An exit from cell cycle control. Nat Rev Cancer 2009;9:785–97.
7. Sachdeva UM, O'Brien JM. Understanding pRb: Toward the necessary development of targeted treatments for retinoblastoma. J Clin Invest. 2012;122:425–34.
8. Dimaras H, Khetan V, Halliday W, Orlic M, Prigoda NL, Piovesan B, Marrano P, Corson TW, Eagle RC, Jr., Squire JA, Gallie BL. Loss of RB1 induces non-proliferative retinoma: Increasing genomic instability correlates with progression to retinoblastoma. Hum Mol Genet. 2008;17:1363–72.
9. Bashyam MD, Animireddy S, Bala P, Naz A, George SA. The yin and yang of cancer genes. Gene 2019;704: 121–33.
10. Lapenna S, Giordano A. Cell cycle kinases as therapeutic targets for cancer. Nat Rev Drug Discov. 2009;8:547–66.
11. Strebhardt K, Ullrich A. Targeting polo-like kinase 1 for cancer therapy. Nat Rev Cancer 2006;6:321–30.
12. Schmucker S, Sumara I. Molecular dynamics of PLK1 during mitosis. Mol Cell Oncol. 2014;1:e954507.
13. Martin BT, Strebhardt K. Polo-like kinase 1: Target and regulator of transcriptional control. Cell Cycle 2006;5:2881–5.
14. Liu Z, Sun Q, Wang X. PLK1, a potential target for cancer therapy. Transl Oncol. 2017;10:22–32.
15. Singh L, Pushker N, Sen S, Singh MK, Chauhan FA, Kashyap S. Prognostic significance of polo-like kinases in retinoblastoma: Correlation with patient outcome, clinical and histopathological parameters. Clin Exp Ophthalmol. 2015;43:550–7.
16. Yim H, Erikson RL. Plk1-targeted therapies in TP53- or RAS-mutated cancer. Mutat Res. 2014;761:31–9.
17. Medema RH, Lin CC, Yang JC. Polo-like kinase 1 inhibitors and their potential role in anticancer therapy, with a focus on NSCLC. Clin Cancer Res. 2011;17:6459–66.
18. Lee KS, Burke TR, Jr., Park JE, Bang JK, Lee E. Recent advances and new strategies in targeting Plk1 for anticancer therapy. Trends Pharmacol Sci. 2015;36:858–77.
19. Ohnuma T, Lehrer D, Ren C, Cho SY, Maniar M, Silverman L, Sung M, Gretz HF, 3rd, Benisovich V, Navada S, Akahoho E, Wilck E, Taft DR, Roboz J, Wilhelm F, Holland JF. Phase 1 study of intravenous rigosertib (ON 01910.Na), a novel benzyl styryl sulfone structure producing G2/M arrest and apoptosis, in adult patients with advanced cancer. Am J Cancer Res. 2013;3:323–38.
20. Navada SC, Silverman LR. The safety and efficacy of rigosertib in the treatment of myelodysplastic syndromes. Expert Rev Anticancer Ther. 2016;16:805–10.
21. Dimaras H, Kimani K, Dimba EA, Gronsdahl P, White A, Chan HS, Gallie BL. Retinoblastoma. Lancet 2012; 379:1436–46.
22. Rao R, Honavar SG, Mulay K, Reddy VAP. Eye salvage in diffuse anterior retinoblastoma using systemic chemotherapy with periocular and intravitreal topotecan. J AAPOS 2018;22:235–7 e232.
23. Xue K, Ren H, Meng F, Zhang R, Qian J. Ocular toxicity of intravitreal melphalan for retinoblastoma in Chinese patients. BMC Ophthalmol. 2019;19:61.
24. Nie C, Ma H, Gao Y, Li J, Tang Z, Chen Y, Lu R. RNA sequencing and bioinformatic analysis on retinoblastoma revealing cell cycle deregulation being a key process in retinoblastoma tumorigenesis. Ophthalmologica 2021;244(1):51–9.

25. Tang Z, Ma H, Mao Y, Ai S, Zhang P, Nie C, Gao Y, Lu R. Identification of stemness in primary retinoblastoma cells by analysis of stem-cell phenotypes and tumorigenicity with culture and xenograft models. Exp Cell Res. 2019;379:110–8.
26. Saengwimol D, Rojanaporn D, Chaitankar V, Chittavanich P, Aroonroch R, Boontawon T, Thammachote W, Jinawath N, Hongeng S, Kaewkhaw R. A three-dimensional organoid model recapitulates tumorigenic aspects and drug responses of advanced human retinoblastoma. Sci Rep. 2018;8:15664.
27. Gutteridge RE, Ndiaye MA, Liu X, Ahmad N. Plk1 inhibitors in cancer therapy: From laboratory to clinics. Mol Cancer Ther. 2016;15:1427–35.
28. Takaki T, Trenz K, Costanzo V, Petronczki M. Polo-like kinase 1 reaches beyond mitosis—Cytokinesis, DNA damage response, and development. Curr Opin Cell Biol. 2008;20:650–60.
29. van de Weerdt BC, Medema RH. Polo-like kinases: A team in control of the division. Cell Cycle 2006;5:853–64.
30. Grinshtein N, Datti A, Fujitani M, Uehling D, Prakesch M, Isaac M, Irwin MS, Wrana JL, Al-Awar R, Kaplan DR. Small molecule kinase inhibitor screen identifies polo-like kinase 1 as a target for neuroblastoma tumor-initiating cells. Cancer Res. 2011;71:1385–95.
31. Gumireddy K, Reddy MV, Cosenza SC, Boominathan R, Baker SJ, Papathi N, Jiang J, Holland J, Reddy EP. ON01910, a non-ATP-competitive small molecule inhibitor of Plk1, is a potent anticancer agent. Cancer Cell 2005;7:275–86.
32. Cheng CY, Liu CJ, Huang YC, Wu SH, Fang HW, Chen YJ. BI2536 induces mitotic catastrophe and radiosensitization in human oral cancer cells. Oncotarget 2018;9:21231–43.
33. Hyoda T, Tsujioka T, Nakahara T, Suemori S, Okamoto S, Kataoka M, Tohyama K. Rigosertib induces cell death of a myelodysplastic syndrome-derived cell line by DNA damage-induced G2/M arrest. Cancer Sci. 2015;106:287–93.
34. Wang Z, Fan M, Candas D, Zhang TQ, Qin L, Eldridge A, Wachsmann-Hogiu S, Ahmed KM, Chromy BA, Nantajit D, Duru N, He F, Chen M, Finkel T, Weinstein LS, Li JJ. Cyclin B1/Cdk1 coordinates mitochondrial respiration for cell-cycle G2/M progression. Dev Cell 2014;29:217–32.
35. Choi M, Kim W, Cheon MG, Lee CW, Kim JE. Polo-like kinase 1 inhibitor BI2536 causes mitotic catastrophe following activation of the spindle assembly checkpoint in non-small cell lung cancer cells. Cancer Lett. 2015; 357:591–601.
36. Wagner EF, Nebreda AR. Signal integration by JNK and p38 MAPK pathways in cancer development. Nat Rev Cancer 2009;9:537–49.
37. Chen Z, Gibson TB, Robinson F, Silvestro L, Pearson G, Xu B, Wright A, Vanderbilt C, Cobb MH. MAP kinases. Chem Rev. 2001;101:2449–76.
38. Low HB, Zhang Y. Regulatory Roles of MAPK phosphatases in cancer. Immune Netw. 2016;16:85–98.
39. Brancho D, Tanaka N, Jaeschke A, Ventura JJ, Kelkar N, Tanaka Y, Kyuuma M, Takeshita T, Flavell RA, Davis RJ. Mechanism of p38 MAP kinase activation in vivo. Genes Dev. 2003;17:1969–78.
40. Tournier C, Hess P, Yang DD, Xu J, Turner TK, Nimnual A, Bar-Sagi D, Jones SN, Flavell RA, Davis RJ. Requirement of JNK for stress-induced activation of the cytochrome c-mediated death pathway. Science 2000;288:870–4.
41. Chapman CM, Sun X, Roschewski M, Aue G, Farooqui M, Stennett L, Gibellini F, Arthur D, Perez-Galan P, Wiestner A. ON 01910.Na is selectively cytotoxic for chronic lymphocytic leukemia cells through a dual mechanism of action involving PI3K/AKT inhibition and induction of oxidative stress. Clin Cancer Res. 2012;18:1979–91.
42. Chang L, Karin M. Mammalian MAP kinase signalling cascades. Nature 2001;410:37–40.
43. Chun AW, Cosenza SC, Taft DR, Maniar M. Preclinical pharmacokinetics and in vitro activity of ON 01910.Na, a novel anti-cancer agent. Cancer Chemother Pharmacol. 2009;65:177–86.
44. Krishnamoorthy RR, Clark AF, Daudt D, Vishwanatha JK, Yorio T. A forensic path to RGC-5 cell line identification: Lessons learned. Invest Ophthalmol Vis Sci. 2013;54:5712–9.
45. Reddy MV, Venkatapuram P, Mallireddigari MR, Pallela VR, Cosenza SC, Robell KA, Akula B, Hoffman BS, Reddy EP. Discovery of a clinical stage multi-kinase inhibitor sodium (E)-2-{2-methoxy-5-[(2',4',6'-trimethoxystyrylsulfonyl)methyl]phenylamino}acetate (ON 01910.Na): Synthesis, structure–activity relationship, and biological activity. J Med Chem. 2011;54:6254–76.
46. Rodriguez-Galindo C, Chantada GL, Haik BG, Wilson MW. Treatment of retinoblastoma: Current status and future perspectives. Curr Treat Options Neurol. 2007;9:294–307.
47. AlAli A, Kletke S, Gallie B, Lam WC. Retinoblastoma for pediatric ophthalmologists. Asia Pac J Ophthalmol. (Phila) 2018;7:160–8.
48. Chawla B, Singh R. Recent advances and challenges in the management of retinoblastoma. Indian J Ophthalmol. 2017;65:133–9.
49. Villegas VM, Hess DJ, Wildner A, Gold AS, Murray TG. Retinoblastoma. Curr Opin Ophthalmol. 2013;24:581–8.
50. Campbell M, Ozaki E, Humphries P. Systemic delivery of therapeutics to neuronal tissues: A barrier modulation approach. Expert Opin Drug Deliv. 2010;7:859–69.
51. Pritchard EM, Dyer MA, Guy RK. Progress in small molecule therapeutics for the treatment of retinoblastoma. Mini Rev Med Chem. 2016;16:430–54.
52. Zhang K, Zhang L, Weinreb RN. Ophthalmic drug discovery: Novel targets and mechanisms for retinal diseases and glaucoma. Nat Rev Drug Discov. 2012;11:541–59.
53. Navada SC, Fruchtman SM, Odchimar-Reissig R, Demakos EP, Petrone ME, Zbyszewski PS, Holland JF, Silverman LR. A phase 1/2 study of rigosertib in patients with myelodysplastic syndromes (MDS) and MDS progressed to acute myeloid leukemia. Leuk Res. 2018;64:10–6.
54. Garcia-Manero G, Fenaux P, Al-Kali A, Baer MR, Sekeres MA, Roboz GJ, Gaidano G, Scott BL, Greenberg P, Platzbecker U, Steensma DP, Kambhampati S, Kreuzer KA, Godley LA, Atallah E, Collins R, Jr., Kantarjian H, Jabbour E, Wilhelm FE, Azarnia N, Silverman LR, investigators Os. Rigosertib versus best supportive care for patients with high-risk myelodysplastic syndromes after failure of hypomethylating drugs (ONTIME): A randomised, controlled, phase 3 trial. Lancet Oncol. 2016;17:496–508.
55. O'Neil BH, Scott AJ, Ma WW, Cohen SJ, Aisner DL, Menter AR, Tejani MA, Cho JK, Granfortuna J, Coveler AL, Olowokure OO, Baranda JC, Cusnir M, Phillip P, Boles J, Nazemzadeh R, Rarick M, Cohen DJ, Radford J, Fehrenbacher L, Bajaj R, Bathini V, Fanta P, Berlin J, McRee AJ, Maguire R, Wilhelm F, Maniar M, Jimeno A, Gomes CL, Messersmith WA. A phase II/III randomized study to compare the efficacy and safety of rigosertib plus gemcitabine versus gemcitabine alone in patients with

previously untreated metastatic pancreatic cancer. Ann Oncol. 2016;27:1180.
56. Bowles DW, Diamond JR, Lam ET, Weekes CD, Astling DP, Anderson RT, Leong S, Gore L, Varella-Garcia M, Vogler BW, Keysar SB, Freas E, Aisner DL, Ren C, Tan AC, Wilhelm F, Maniar M, Eckhardt SG, Messersmith WA, Jimeno A. Phase I study of oral rigosertib (ON 01910.Na), a dual inhibitor of the PI3K and Plk1 pathways, in adult patients with advanced solid malignancies. Clin Cancer Res. 2014;20:1656–65.
57. O'Neil BH, Scott AJ, Ma WW, Cohen SJ, Leichman L, Aisner DL, Menter AR, Tejani MA, Cho JK, Granfortuna J, Coveler AL, Olowokure OO, Baranda JC, Cusnir M, Phillip P, Boles J, Nazemzadeh R, Rarick M, Cohen DJ, Radford J, Fehrenbacher L, Bajaj R, Bathini V, Fanta P, Berlin J, McRee AJ, Maguire R, Wilhelm F, Maniar M, Jimeno A, Gomes CL, Messersmith WA. A phase II/III randomized study to compare the efficacy and safety of rigosertib plus gemcitabine versus gemcitabine alone in patients with previously untreated metastatic pancreatic cancer. Ann Oncol. 2015;26:1923–9.